

---

# Data Reduction and Analysis of the M35 Open Stellar Cluster

## Laboratory Report, Observational Astrophysics I

Ángela Abad Martín

March, 2024

Professors: Angela Adamo, Adrianus Bik and Giacomo Bortolini

### **Abstract**

Observational astronomy allows, through the use of telescopes, astronomical devices and digital programs, the exploration of celestial bodies and the examination of their characteristics and peculiarities. The primary objective along this project is to develop computational codes within the `Python` program, as well as the implementation of the `SAOImageDS9` tool, aimed at analyzing the data pertaining to the open stellar cluster M35.

From an observation taking place on February the 22nd of 2024 with the Telescope 21 of the Utah Desert Remote Observatory, an estimation of the cluster's age has been calculated, obtaining  $\log(t_{age}) \approx [7.699, 8.477]$  by analyzing the position of the turn-off point and the distribution of some of its stars in the Hertzsprung-Russell (HR) diagram. To do so, photometric techniques were applied using B and V filters, characterizing apparent and absolute magnitudes ( $m$  and  $M$ ) as well as stellar intrinsic colors ( $(B - V)_{int}$ ) and effective temperatures ( $T_{eff}$ ).

As a result, it has been concluded that the cluster is a relatively young source with most of its stars remaining along the main sequence according to the analyzed data.

# Contents

<b>1</b>	<b>Introduction</b>	<b>1</b>
<b>2</b>	<b>Observations</b>	<b>1</b>
2.1	Technical Justification . . . . .	1
2.2	Calibration Files . . . . .	2
2.2.1	Bias Files . . . . .	2
2.2.2	Dark Files . . . . .	2
2.2.3	Flat Files . . . . .	2
2.3	Exposure time . . . . .	3
<b>3</b>	<b>Data Reduction</b>	<b>3</b>
3.1	Master Bias . . . . .	3
3.2	Master Dark . . . . .	4
3.3	Master Flats . . . . .	4
3.4	Acquisition of the Science Frames . . . . .	4
<b>4</b>	<b>Analysis</b>	<b>5</b>
4.1	Aperture Analysis . . . . .	5
4.2	Count Extraction and Flux Determination . . . . .	7
4.3	Colors ((B – V)), Effective Temperatures ( $T_{\text{eff}}$ ) and Magnitudes (m and M) . . . . .	8
<b>5</b>	<b>Result: HR Diagram</b>	<b>10</b>
<b>6</b>	<b>Conclusions</b>	<b>11</b>
	<b>References</b>	<b>12</b>

# 1 Introduction

Stellar evolution studies are crucial when determining the internal properties and development stage of stars. Throughout this project, the open stellar cluster M35 (an intermediate-age open cluster in the direction of the Galactic anti-centre ( $\alpha = 6h\ 8m\ 56.5s$ ,  $\delta = 24^\circ\ 21.6'$ ), [9]) is analyzed with the main objective of obtaining an estimation of its age. This cluster is located at a distance of  $d = 734.17$  pc (with a distance modulus of  $\mu = 9.329$ ) and is characterized by presenting around 500 stars [4, 5].

Starting by assuming a “coeval” scenario (meaning that all stars are approximately formed simultaneously), a suitable approach for characterizing the age of the cluster consists of determining its Hertzsprung-Russel (HR) diagram associated to a population of 40 selected stars. This can be achieved by the representation of the absolute magnitude in the V band ( $M_V$ ) for the stars and their corresponding intrinsic colors ( $(B - V)_{int}$ ) (see Sections 4 and 5). Thereafter, an analysis of the turn-off point (position where the most massive star resides within the Main Sequence (MS)) is required by elaborating some isochrone fitting, offering insight into the cluster’s age [5].

Consequently, photometric techniques are essential in order to conduct a correct procedure. To begin with, the measurement of the cluster using two different filters (B and V) is necessary to obtain the star’s surface brightness and thus associated apparent magnitudes ( $m_B$  and  $m_V$ , respectively). This leads to an analysis from which the colors and temperatures of the stars can be calculated, as well as the absolute magnitudes, driving to the elaboration of the desired diagram [1].



**Figure 1:** Graphic representation of the FOV of T21 in comparison with the apparent size of M35. [Figure retrieved from [10]].

## 2 Observations

### 2.1 Technical Justification

The planning for performing the observation was initially established for February the 21st of 2024, from the Utah Desert Remote Observatory (USA) by using Telescope 21 (T21). However, the actual date had to be delayed to February the 22nd of 2024 due to purely climatological reasons since not only the visibility plot was much more convenient (the cluster reached its culmination point within the first night hours without a direct contribution from the moon), but the weather forecast was stated as being “good” with “excellent” seeing.

On the other hand, the motivation behind the selection of the telescope relies on it being characterized by having a Field of View (FOV) of  $(0.81 \times 0.54)$  deg., fitting perfectly with the apparent size

of M35 ( $\approx 28$  arcmin, [3]) (see Figure 1). Additionally, it presented the B and V filters needed for the analysis procedure and met visibility requirements as it is located in the Northern hemisphere [1, 7].

## 2.2 Calibration Files

During the process of observing astronomical bodies, a series of raw data is collected, where the presence of background noise as well as the noise coming from the optics of the instrument must be considered and suppressed through data reduction techniques (see Section 3). Throughout this section, the basic three types of noise are presented, as well as the way they were selected for the project's purpose.

### 2.2.1 Bias Files

When photons with sufficient energy reach the pixels in the CCD (Charge-Coupled Device) of a telescope, they can excite and store photoelectrons in them. Then, starting in a certain pixel, a voltage signal counts the amount of photoelectrons stored, it clears them and shifts all the photoelectrons of the contiguous pixels to their adjacent cells to continue the counting process. In reality, however, some electrons may be left behind during the shifting procedure, causing a trail in the raw image that may not belong to the actual morphology of the source.

These errors are called "bias" and are images that only contain read noise, so they are taken with zero exposure time and with the telescope covered so that only the CCD is read. For this observation, a selection of 10 bias files was gathered from [6].

### 2.2.2 Dark Files

Due to electrical currents and wiring beneath the CCD, electron excitations occur as a result of thermal effects, leading to an excessive count of electrons in pixels that manifests as background noise, which escalates with rising temperatures and with the duration of the telescope's exposure time.

Referred to as "dark" noise, this phenomenon is measured with the telescope covered and must have the same exposure time as the source under investigation. While searching for the best dark files in [6], it was challenging to find those with the same time exposures as the desired source images (only files with a time exposure of 900s were found, from which 10 were selected). In order to correct for the time exposure needed during the reduction process, a linear relationship was applied (see Section 3).

### 2.2.3 Flat Files

Sometimes there is noise originating from the inhomogeneities of the lenses and the uneven illumination caused by dust or stains in the optical path, intimately related to the sensor's quantum efficiency [8]. This manifests as vignetting in the corners or as "donut-shaped" spots and is referred to as "flat" files. They are captured with the same exposure time as the source and with the telescope aperture open.

Each flat file is measured per filter used. This way, two files were selected from [6], one in the V filter with exposure time of  $\approx 6.903$ s and another one in the B filter with exposure time of  $\approx 8.127$ s. Although it would have been more convenient to select multiple files (as happened with the dark and bias frames), in this case it was impossible to find any further ones.

### 2.3 Exposure time

Before proceeding with the observation, a brief and intuitive analysis regarding the total time needed for the observation of the source is presented.

Since B and V filter frames had to be taken for an accurate photometric analysis, as well as long and short time displays in favor of an optimistic detection of the faintest and brightest stars, respectively [1], the following selection was done (see Table 1).

$t_{\text{exp}} = 50\text{s}$	$t_{\text{exp}} = 160\text{s}$	$t_{\text{exp}} = 260\text{s}$
$B_{\text{filter}}$ (1 frame)	$B_{\text{filter}}$ (1 frame)	$B_{\text{filter}}$ (1 frame)
$V_{\text{filter}}$ (1 frame)	$V_{\text{filter}}$ (1 frame)	$V_{\text{filter}}$ (1 frame)

**Table 1:** Selection of exposure times and filters.

As we can see, this resulted in a total of 6 frames. Additionally, since the calibration files were obtained from [6], there was no need to reserve observation time for their acquisition, meaning that the only time needed corresponded to the measurement of the source's frames, as can be seen in the following expression,

$$t_{\text{obs,tot}} = 2 \cdot (50 + 160 + 260) \cdot 1.5\text{s} = 23.5\text{min} \quad (1)$$

where the 1.5 factor was purposely added, accounting for possible errors, delays or even additional time required during the procedure in case of inconvenience [1].

## 3 Data Reduction

Before proceeding with the correction of the 6 raw source frames, it was necessary to obtain what astronomers call "master files" for each of the three types of errors described in Section 2.2. They consist of an averaged combination of the individual files with the aim of subtracting the noise from the raw images more effectively and accurately, obtaining final "science frames".

### 3.1 Master Bias

The master bias can easily be obtained by averaging the individual bias frames as follows:

$$MB = \frac{1}{n_B} \sum_i^{n_B} B_i \quad (2)$$

where  $n_B$  represents the number of individual bias frames used ( $n_B = 10$  in this project) and  $B_i$  indicates the data from each individual bias frame.

Computationally, this was achieved generating a 3D array in which each layer ( $x$  and  $y$  directions) belonged to an individual bias frame and they were all organized one after the other along the  $z$  direction. The `np.nanmean` function was applied along this latter direction in order to do the average avoiding the "not a number" values during the process. In Figure 2 (a), the representation of the master bias can be seen (containing a couple of hot pixels, probably due to charge leakage).

### 3.2 Master Dark

For obtaining the master dark, a similar procedure to the one described above is implemented, taking into account that it had to be corrected for the master bias,

$$MD = \left( \frac{1}{n_D} \sum_i^{n_D} D_i \right) - MB = MD_{noise} - MB \quad (3)$$

Here, again,  $n_D$  represents the number of individual dark frames used ( $n_D = 10$ ) and  $D_i$  indicates the data from each individual dark frame. By averaging them as done in Eq.(2), a "master dark with noise" is obtained ( $MD_{noise}$ ), the one from which the master bias ( $MB$ ) is subtracted (see Figure 3 (b) for a visual representation, showing hot pixels due to electrical noise).

This expression is applied for  $t_{exp} = 900s$  dark frames obtained in Section 2.2.2 ( $MD_{t_{exp}=900s}$ ). However, different master darks should be generated for different exposure times as each raw source frame should be calibrated with the master file associated to its individual exposure time. Since it was impossible to find any dark frames with  $t_{exp} = 50s$ ,  $t_{exp} = 160s$  or  $t_{exp} = 260s$ , a simple formula which assumes a linear tendency was applied,

$$\frac{MD(t_{exp} = 900s)}{t_{exp} = 900s} = \frac{MD(t_{exp} = 50s)}{t_{exp} = 50s} = \frac{MD(t_{exp} = 160s)}{t_{exp} = 160s} = \frac{MD(t_{exp} = 260s)}{t_{exp} = 260s} \quad (4)$$

### 3.3 Master Flats

In the case of master flats, as previously stated, it is necessary to generate one per filter. Each flat field, as read out from the CCD, contains a bias and has some dark current ([4]), so it is necessary to subtract them both. Since no master darks with the same exposure time as the flats were selected in Section 2.2.3, it was necessary to generate new ones by using Eq.(4).

Once corrected, the flats had to go through a normalization process in the  $x$  and  $y$  directions before constructing the master files (this was done to re-scale the results and thus obtain a consistent value for pixels with higher luminosity). See Figure 2 (c) for an example of a master flat in the V filter for a time exposure of 6.903s; notice the "donut-shape" areas and vignetting).

$$MF_i = \frac{F_i(t_{exp}) - MB - MD(t_{exp})}{\langle F_i(t_{exp}) - MB - MD(t_{exp}) \rangle} \quad (5)$$

In Eq.(5) we can see that the master flat obtained ( $MF_i$ ) is per flat file analyzed ( $F_i(t_{exp})$ ), which in this case was simply one per filter ( $i = 1$ ) as it was not possible to find more for the same filter and time exposures.

However, the more flat files you analyze, the better correction you can apply and a further step would take place: normalizing again the array of  $MF_i$  in the  $z$  direction. In this case it is not necessary since only one flat file was obtained per filter.

### 3.4 Acquisition of the Science Frames

Once the master files have been characterized, the next step consists on correcting the raw frames ( $RF$ ) belonging to the source so as to finally obtain the science frames ( $SF$ ) needed to continue with

the analysis of data (see Eq.(6)). We must emphasize the importance of using the same exposure times and filters during the analysis of each image, making use of the Eq.(4) whenever necessary.

$$SF(t_{exp}, filter) = \frac{RF(t_{exp}, filter) - MB - MD(t_{exp})}{MF(t_{exp}, filter)} \quad (6)$$

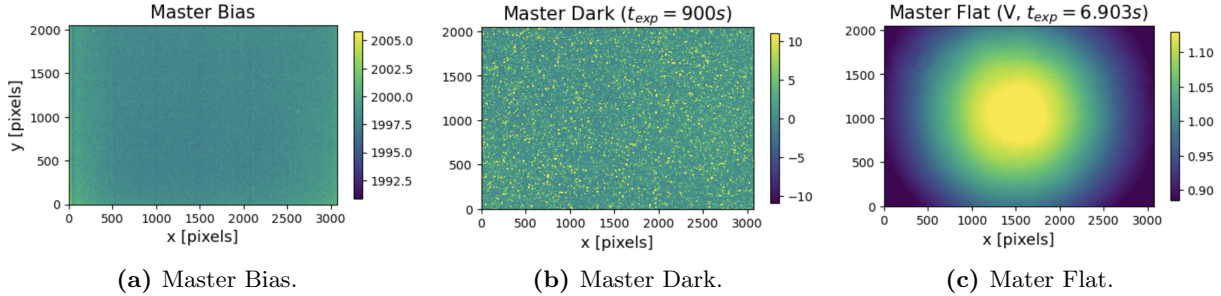


**Figure 2:** Exemplification of some master files obtained during the data reduction process. [Figures retrieved from personal code via Python].

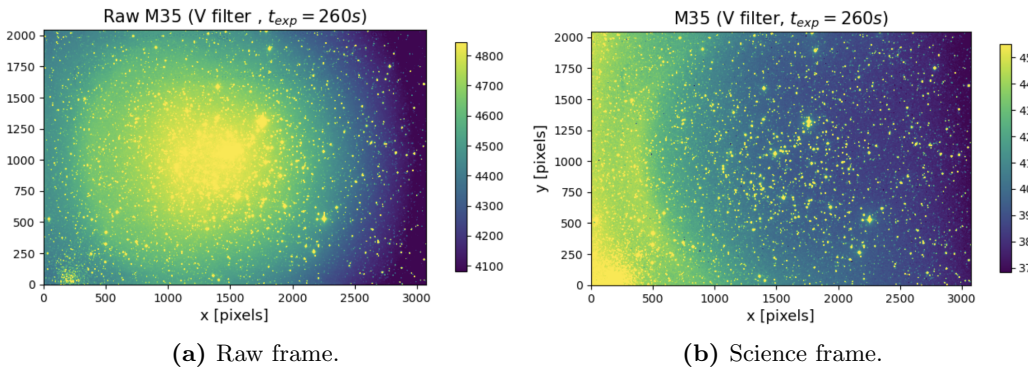


**Figure 3:** Comparison of a raw and science frame for a time exposure of 260s in the V filter to show the efficiency of the reduction process. [Figures retrieved from personal code via Python].

## 4 Analysis

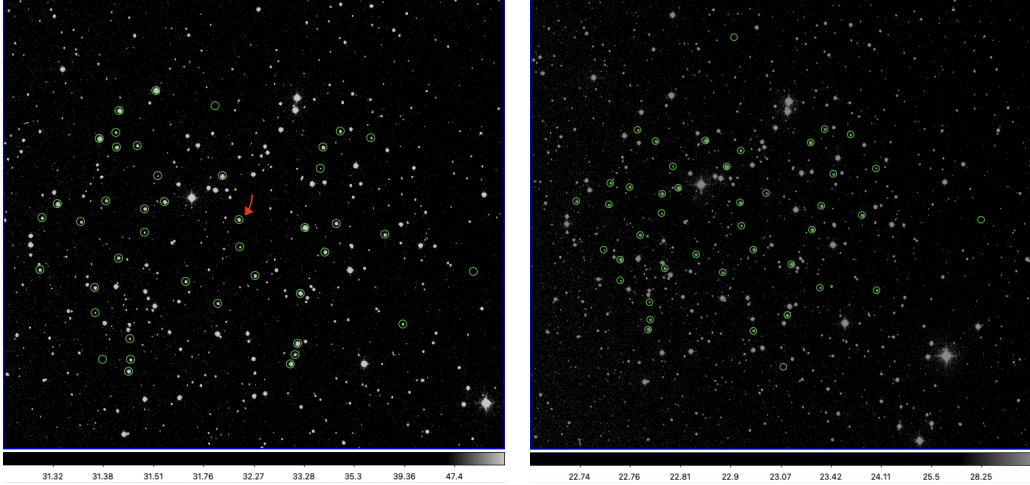
The process of estimating the age of the open stellar cluster M35 involves a series of photometric and computational analysis dealing with astronomical parameters.

### 4.1 Aperture Analysis

Now that the science images have already been calibrated, the process continues by opening each of the 6 corrected files into the astronomical tool `SAOImageDS9`. In here, it is necessary to firstly select a good number of stars for the subsequent execution of the HR diagram (in this case 40 were chosen, including the calibration star, necessary for the following magnitude analysis). Additionally, 3 sky apertures had to be elected for a subsequent correction of the extracted counts in each star.

The size of the apertures were the same in all the images in order to avoid further complications and the selection of the different regions varied for each time exposure due to issues associated to the saturation of pixels for larger exposure times. However, the location of the apertures were fixed

withing the same time exposure for the two filter images and no rolling was required since they were accurately aligned, fitting the star's positions precisely.



(a) M35 in the B filter with  $t_{exp} = 50s$  (red arrow points to the calibration star, determined by Figure 8 in [[5]]). (b) M35 in the B filter with  $t_{exp} = 260s$ . Some new regions selected.

**Figure 4:** Comparison of the apertures selection (40 stars and three sky regions) for the same science frame in the B band: (a)  $t_{exp} = 50s$ , (b)  $t_{exp} = 260s$ . [Figures retrieved from personal data via SAOImageDS9.]

The size of the apertures had to be broad enough to fit in the brightest non-over-saturated stars in each science frame so as to get the same amount of the PSF (Point Spread Function) for each star [4]]. Along the project's instructions ([5]), an estimation of the seeing is asked. It is known, from the course's lectures ([8]), that an approximate value for the seeing can be determined out of the Full Width Half Maximum (FWHM) of the PSF. To do so, the projection of a bright yet non-saturated star is analyzed using SAOImageDS9 in the B and V filters for a  $t_{exp} = 50s$ . By measuring that projection several times for the same star (allowing for statistical results), the value for the FWHM is estimated by counting the number of pixels it covers at haft maximum (see Figure 5 for an example). Those results are combined by executing their mean value (Eq. (7), where  $x_i$  indicated the individual results and  $N$  the total number of values examined)

$$\bar{x} = \frac{\sum_{i=1}^N x_i}{N} \quad (7)$$

and then computing their standard deviation (Eq. (8)) and consequent uncertainty of the mean (Eq. (9)) [8]

$$s = \sqrt{\frac{1}{N-1} \sum_{i=1}^N (x_i - \bar{x})^2} \quad (8)$$

$$\sigma_{\bar{x}} = \frac{s}{\sqrt{N}} \quad (9)$$

Once the widths in pixels are determined ( $\text{FWHM}_B = (2.67 \pm 0.17)$ pixels and  $\text{FWHM}_V = (3.5 \pm 0.29)$ pixels), the last step consists on multiplying them by the resolution of the telescope (0.96 arcsec/pixel, [10]) obtaining that the seeing is  $(2.56 \pm 0.17)$ arcsec for the B band and  $(3.36 \pm 0.29)$ arcsec for the V band, suggesting that despite not being excellent, the astronomical conditions were moderate during image acquisition. Also, the fact that the seeing for the V filter is larger than for the B already suggests the poorer quality of the images in the more visible part of the spectrum due to a possible reddening and to the fact that stars may be bluer (younger) (see Sections 4.3 and 5).

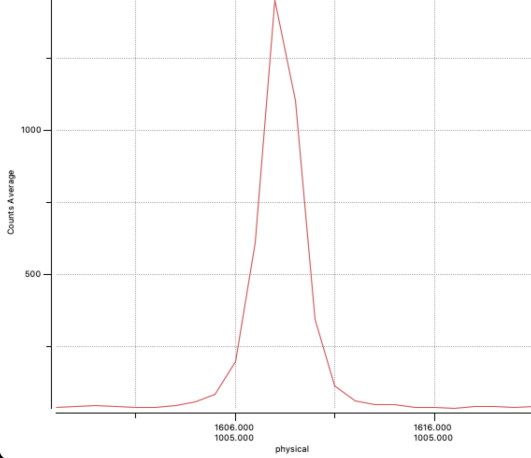


**Figure 5:** Exemplification of the PSF for a star to measure its FWHM. [Figure retrieved from personal data via SAOImageDS9].

Although this procedure had to be repeated for each filter in each exposure time so as to obtain a more precise evaluation, since it was merely an estimation and due to the lack of time it was kept this way.

## 4.2 Count Extraction and Flux Determination

After saving the three different aperture files for each time exposure, the corresponding positions and radius of the regions were read and saved using the Python function `regeextract`. Next step consisted on deriving the counts belonging to those apertures, for both the stars and the sky regions in each filter per exposure time. By using the Python function `aper` and introducing the position and radius of the pertinent areas, the associated fluxes and fluxes errors were determined. Subsequently, the evaluation of the stars' fluxes through sky calibration was executed by using the following general expression:

$$F_{\star} = F_{\star,raw} - \frac{F_{sky} \cdot A_{\star}}{A_{sky}} \quad (10)$$

where  $F_{\star,raw}$  represents the raw fluxes belonging to each selected star,  $F_{sky}$  is the flux associated to the sky region and  $A = \pi r^2$  is the area of the aperture for the star ( $A_{\star}$ ) and the sky ( $A_{sky}$ ). Since the same aperture size was used throughout the whole process ( $A_{\star} \equiv A_{sky}$ ), Eq.(10) and its associated uncertainty reduce to:

$$F_{\star} = F_{\star,raw} - F_{sky} \quad (11)$$

$$\delta F_{\star} = \delta F_{\star,raw} + \delta F_{sky} \quad (12)$$

Additionally, 3 different sky areas were selected in each aperture file to improve the quality of the results. Therefore, the mean of the three was computed (Eq.(7)) to obtain general sky regions.

### 4.3 Colors ((B – V)), Effective Temperatures (T<sub>eff</sub>) and Magnitudes (m and M)

The HR diagram consists on the representation of a series of astronomical parameters to graphically show the different stellar evolutionary phases. It can either be illustrated as the absolute magnitude in the V band ( $M_V$ ) of a group of stars against their intrinsic color ( $(B-V)_{int}$ ) or their luminosity in the V band ( $L_V$ ) versus their effective temperatures ( $T_{eff}$ ) (the V band selection is pure convention). During this project, the former is used, although the calculation of the effective temperatures is carried out as well.

The first stage regarding the manipulation of data consists on the determination of the intrinsic colors of the stars for the frames in each exposure time. The color for an astronomical object is defined as the subtraction of two of its apparent magnitudes ( $m$ ) in different filters (in this case, the B and V). Intrinsic colors are needed since reddening effects in the form of an extinction factor ( $E(B-V)$ ) induced by the interstellar medium between the source and the observer must be taken into account [manual]. Initially, observed colors are calculated out of the calibrated images as:

$$(B - V)_{obs,\star} \equiv m_{B,\star}^{obs} - m_{V,\star}^{obs} \quad (13)$$

$$\delta(B - V)_{obs,\star} = \delta m_{B,\star}^{obs} + \delta m_{V,\star}^{obs} \quad (14)$$

with the observed apparent magnitudes and their associated errors (computed out of propagation methods) defined as

$$m_{filter,\star}^{obs} = m_{filter,calib}^{obs} - 2.5 \cdot \log_{10} \left( \frac{F_{filter,\star}^{obs}}{F_{filter,calib}^{obs}} \right) \quad (15)$$

$$\delta m_{filter,\star}^{obs} = \left| \frac{-2.5}{\ln(10) \cdot F_{filter,\star}^{obs}} \right| \delta F_{filter,\star}^{obs} + \left| \frac{2.5}{\ln(10) \cdot F_{filter,calib}^{obs}} \right| \delta F_{filter,calib}^{obs} \quad (16)$$

According to Eq.(15),  $m_{filter,\star}^{obs}$  and  $F_{filter,\star}^{obs}$  represent the observed apparent magnitude and flux of a certain star in a particular filter while  $m_{filter,calib}^{obs}$  and  $F_{filter,calib}^{obs}$  indicate the observed apparent magnitude and flux of the calibration star (see Figure 4 (a)) in that same filter. In the case of M35,  $m_{B,calib}^{obs} = 11.68$  mag and  $m_{V,calib}^{obs} = 11.40$  mag [3].

Therefore, the first step that had to be executed was the computation of  $m_{V,\star}^{obs}$  and  $m_{B,\star}^{obs}$  for each star in each filter and exposure time, as well as their errors (Eqs.(15) and (16)). Then, the corresponding observed colors were calculated (Eqs.(13) and (14)) and finally the required intrinsic colors and their errors were computed through Eqs. (17) and (18), with  $E(B - V) = 0.2$  mag for M35 ([5]).

$$(B - V)_{int,\star} = (B - V)_{obs,\star} - E(B - V) \quad (17)$$

$$\delta(B - V)_{int,\star} = \delta(B - V)_{obs,\star} \quad (18)$$

Next step consists on the evaluation of the effective temperatures for each star (see Figure 6 for an example) by applying the relations found by [2]

$$T_{eff,\star} = \frac{5040}{\theta_{eff,\star}} \quad (19)$$

$$\theta_{eff,\star} = 0.541 + 0.533 \cdot (B - V)_{int,\star} + 0.007 \cdot (B - V)_{int,\star}^2 \quad (20)$$

and their corresponding propagated uncertainties

$$\delta T_{eff,\star} = \left| \frac{-5040}{\theta_{eff,\star}^2} \right| \delta \theta_{eff,\star} \quad (21)$$

$$\delta \theta_{eff,\star} = |0.533 + 2 \cdot 0.007(B - V)_{int,\star}| \delta(B - V)_{int,\star} \quad (22)$$

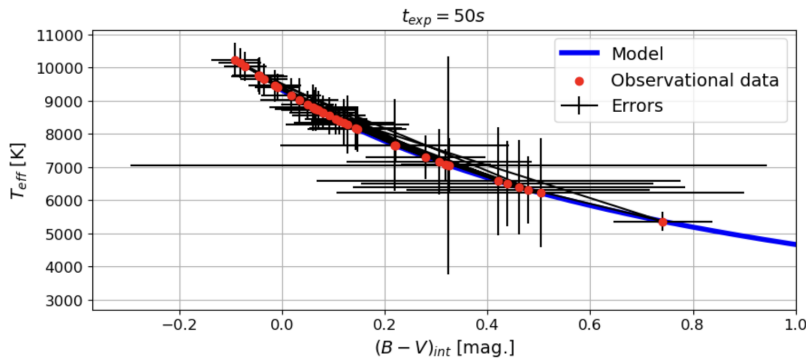


**Figure 6:** Representation of the effective temperatures ( $T_{eff}$ ) of stars and their corresponding intrinsic colors ( $(B - V)_{int}$ ) for a time exposure of  $t_{exp} = 50$ s. Analogous results are obtained for the rest of exposure times and the model is given by Eq.(20) for a range in colors going from [0, 2] magnitudes. [Figure retrieved from personal code via Python].

The final procedure prior to executing the HR diagram consists on the computation of the absolute magnitudes within the V band for the stars ( $M_{V,\star}$ ) in each exposure time frame. Knowing the distance modulus ( $\mu$ ) for M35 (see Section 1) and that it is related to the stars' magnitudes through

$$M_{V,\star} = m_{V,\star} - \mu \quad (23)$$

with the corresponding uncertainties,

$$\delta M_{V,\star} = \delta m_{V,\star} \quad (24)$$

the desired values can be easily obtained.

## 5 Result: HR Diagram

Ultimately, the last step comprises the representation of the absolute magnitudes (Eq. (23)) against the intrinsic colours for the stars (Eq. (17)) in each exposure time (see Figure 7).

As can easily be observed, most of the selected stars seem to be displaced along the main sequence, showing a rather young stellar population without a clear turn off point (although it could potentially be placed around  $M_V \approx 1.5$  and  $(B - V)_{int} \approx 0$ , but this is merely a visual approximation). Some stars can also be detected as scattered from that main sequence, considering a plausible selection of stars not belonging to the cluster itself. Additionally, some lie around the same position in the diagram, meaning that they are the same star analyzed withing the three time exposures. The reason of this is because during the analysis, the selection of stars varied from one exposure time to another for the sake of diagram completeness and to avoid CCD saturation effects. However, many stars were repeated throughout the process to facilitate it, and in the case of the calibration star, to proceed with the conversion of observations into physical parameters. A mean statistical analysis combining the results from all three exposure times could have been executed for a more precise result. Nevertheless, due to the lack of time to proceed properly, it was decided to omit this part.

On the other hand, a fitting process was executed, representing the most accurate isochrones matching the evolutionary trajectory of the stars in the cluster. Although the curves are not perfectly aligned with the observational data, it seems intuitive and consistent to indicate that the cluster's age is around  $\log(t_{age}) \in [7.699, 8.477]$ . Comparing this to the tabulated value stated in [9],  $\log(t_{age})_{tab.} = 8.3 \pm 0.3$ , it can be concluded that a result has been reached with considerable accuracy taking into account the difficulty involved while trying to obtain high-quality observational data, along with the execution of a consistent analysis. This can be seen through the error bars obtained during the project, which tend to have a propensity to be quite substantial as astronomical data is relatively difficult to be measured with rigorous precision (for instance, the faintest sources have the largest error bars, see Figure 7).

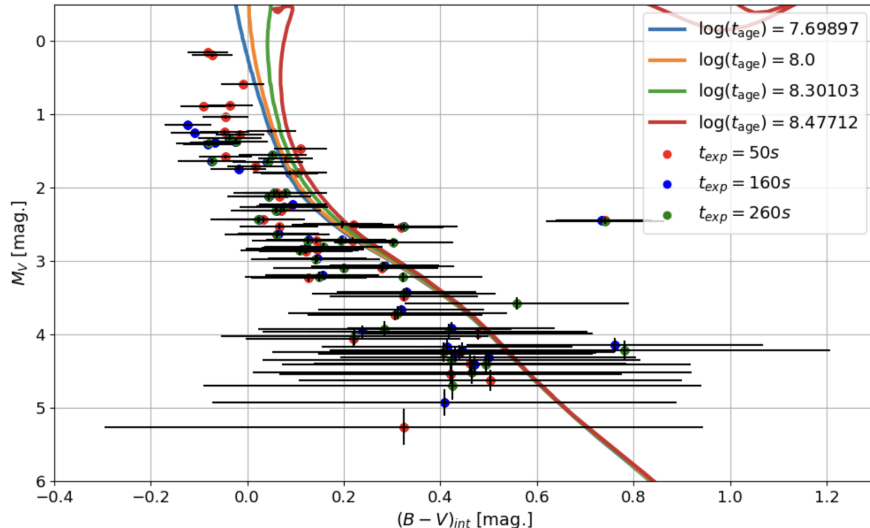


**Figure 7:** HR diagram for the stars analyzed in each exposure time. Four isochrones have been fitted to argument the estimated age of the open cluster. [Figure retrieved from personal code via Python.]

## 6 Conclusions

During the elaboration of this project, the open stellar cluster M35 was observationally detected using photometric techniques in an attempt to estimate its age with the fitting of isochrones along the HR diagram.

The process started with the measurement of 6 different frames in both the B and V filters and for exposure times of 50, 160 and 260s by using the remote iTelescope T21 belonging to the Utah Desert Remote Observatory [10]. Subsequently, the compilation of different bias, dark and flat frames from [6] allowed for their later conversion into master files, applied during the reduction process where science frames were finally generated.

Next step consisted on the selection of different aperture regions along the images in order to be able to analyze 40 stars and 3 sky areas. Through computational processes (via the use of `Python` and `SAOImageDS9`) and the implementation different functions, their corresponding fluxes were obtained, out of which the following astronomical parameters were progressively calculated: apparent stellar magnitudes (Eq.(15)), intrinsic colors (Eq.(17)), effective temperatures (Eq.(19))and absolute stellar magnitudes (Eq.(23)).

Finally, the HR diagram associated to the selected stars belonging to M35 was represented (see Figure 7), showing an estimated age for the cluster:  $\log(t_{\text{age}}) \in [7.699, 8.477]$ , positively agreeing with tabulated values such as that of [9] ( $\log(t_{\text{age}}) = 8.3 \pm 0.3$ ) and confirming a consistent computational and mathematical execution of the analysis.

As can be seen, M35 could be considered a relatively young source, with most of its stars (at least the ones selected) gathered along the main sequence. These are also younger because they can be seen as bluer during the seeing analysis, where it was found that the quality of the images was improved withing the B filter, giving relevance to the extinction effects of the interstellar medium.

## References

1. Abad Martín, Á. *Examination of the Open Stellar Cluster M35 to Uncover its Physical Properties* Observational Astrophysics I Proposal. 2024.
2. Alonso, A., Arribas, S. & Martinez-Roger, C. The empirical scale of temperatures of the low main sequence (F0V-K5V). *Astronomy and Astrophysics*, v. 313, p. 873-890 **313**, 873–890 (1996).
3. Bortolini, G. *Data Reduction and Analysis* Observational Astrophysics I, Laboratory. 2024.
4. Bortolini, G. *Python Programming Code*: Datareduction<sub>obs12024.ipynb</sub>. 2024.
5. Gålfalk, M. Observational Astrophysics I. Laboratory exercise manual-HR diagram of a cluster. *Athena*. Updated by Alex Pietrow, Gayathri Viswanath and Giacomo Bortolini (2024).
6. itelescope.net. <https://data.itelescope.net>.
7. *Overview of all Telescopes* <https://support.itelescope.net/support/solutions/articles/247371-overview-of-all-telescopes>.
8. R. Chrome, F. *To Measure the Sky. An Introduction to Observational Astronomy* (Cambridge University Press, 2016).
9. Sung, H. & Bessell, M. UBV CCD photometry of M35 (NGC 2168). *Monthly Notices of the Royal Astronomical Society* **306**, 361–370 (1999).
10. *Telescope 21*. [https://support.itelescope.net/support/solutions/articles/231906-telescope-21?utm\\_source=Telescopius&utm\\_medium=link&utm\\_campaign=TelescopeSimulator](https://support.itelescope.net/support/solutions/articles/231906-telescope-21?utm_source=Telescopius&utm_medium=link&utm_campaign=TelescopeSimulator).